JACS
JOURNAL OF THE AMERICAN CHEMICAL SOCIETY
Communication
pubs.acs.org/JACS

Decoupling the Electrical Conductivity and Seebeck Coefficient in the RE_2SbO_2 Compounds through Local Structural Perturbations

Peng L. Wang,[†] Taras Kolodiazhnyi,[‡] Jinlei Yao,[†] and Yurij Mozharivskyj*,[†]

[†]Department of Chemistry and Chemical Biology, McMaster University, 1280 Main Street West, Hamilton, Ontario, Canada L8S 4M1

[‡]National Institute for Materials Science, 1-1 Namiki, Tsukuba, Ibaraki, 305-0044 Japan

Supporting Information

ABSTRACT: Compromise between the electrical conductivity and Seebeck coefficient limits the efficiency of chemical doping in the thermoelectric research. An alternative strategy, involving the control of a local crystal structure, is demonstrated to improve the thermoelectric performance in the RE_2SbO_2 system. The RE_2SbO_2 phases, adopting a disordered *anti*-$ThCr_2Si_2$-type structure ($I4/mmm$), were prepared for *RE* = La, Nd, Sm, Gd, Ho, and Er. By traversing the rare earth series, the lattice parameters of the RE_2SbO_2 phases are gradually reduced, thus increasing chemical pressure on the Sb environment. As the Sb displacements are perturbed, different charge carrier activation mechanisms dominate the transport properties of these compounds. As a result, the electrical conductivity and Seebeck coefficient are improved simultaneously, while the number of charge carriers in the series remains constant.

The efficiency of a thermoelectric material can be denoted by the dimensionless figure-of-merit, $ZT = \alpha^2\sigma T/k$. A high-efficiency thermoelectric material should possess a large Seebeck coefficient (α) and high electrical conductivity (σ) while exhibiting low thermal conductivity (κ).[1] Chemically increasing the carrier concentration in a degenerate semiconductor generally improves its electrical conductivity since electrical conductivity, σ, is directly proportional to a carrier concentration, n, through $\sigma = ne\mu$.[2] However, the Seebeck coefficient (α) is typically compromised in the process as it is inversely related to the carrier concentration, $a = (8\pi^2k_B^2/3eh^2)mT(\pi/3n)^{3/2}$.[2] These relationships represent limitations of chemical doping for optimizing the power factor, $\alpha^2\sigma$. Many research attempts have been undertaken to achieve a higher-power factor by increasing one of the two parameters while keeping the other one constant.[3] However, similar results are rarely realized in homogeneous bulk materials through a chemical manipulation. In this work, we explore the possibility of improving the power factor in a system by chemically altering the charge carrier transport mechanism rather than by optimizing the carrier concentration.

The recent work on the rare earth bismuthide oxides, RE_2BiO_2, can be considered as an excellent example of the chemical perturbation of transport properties without modifying the number of charge carriers.[4] The RE_2BiO_2 phases undergo a Mott-type insulator-to-metal transition as larger, early, rare earth atoms are replaced by smaller, late, rare earth elements. Such behavior was rationalized in terms of increasing chemical pressure on the square Bi lattice: the Bi−Bi distances decrease as the size of the *RE* atoms becomes smaller and, as a result, the metallic character of the Bi electronic band becomes dominant due to a better Bi−Bi orbital overlap.[4]

Inspired by this study, we have focused our attention on the antimony analogues, RE_2SbO_2 (*RE* = rare earth elements). The high-purity RE_2SbO_2 samples were prepared for *RE* = La, Nd, Sm, Gd, Ho, and Er. First, the corresponding *RE*Sb precursors were prepared from elemental rare earth metals (99.9 wt %) and antimony (99.999 wt %) following the previously reported synthetic route.[5] The *RE*Sb binaries, powdered Sb metal and corresponding RE_2O_3 powder (99.99 wt %, prefired at 1273 K for 12 h), were mixed in the stoichiometric ratios and pressed into 0.5-g pellets in an Ar-filled glovebox. Subsequently, the cold-pressed pellets were sealed in Ta tubes and sintered in a high-frequency induction furnace. After sintering at 1773 K for 16 h, black pellets were obtained. The samples were subjected to X-ray powder diffraction analysis on a PANalytical X'Pert Pro diffractometer with an X'Celerator detector and the Cu $K_{\alpha1}$ radiation. Diffraction data were collected in the 20−70° 2θ range. A full-profile Rietveld refinement (Rietica program[6]) was used to refine the lattice constants and assess the purity of the bulk products. X-ray single-crystal diffraction studies were performed on the extracted crystals. Room-temperature diffraction data were collected on a STOE IPDSII diffractometer with the Mo K_α radiation in the whole reciprocal sphere. Structural determinations and refinements of all the data sets were performed using the SHELXL program.[7]

The RE_2SbO_2 compound with Ce was first reported to adopt the *anti*-$ThCr_2Si_2$ type structure with the $I4/mmm$ space group.[8] As shown in Figure 1, left, the structure consists of alternating RE_2O_2 layers and Sb layers, and each antimony atom on the 2*a* atomic site is surrounded by 8 *RE* atoms. However, a recent study by Nuss and Jansen[9] proposed a modified structural model, in which the Sb atoms were shifted away from the ideal 2*a* position along the *a* direction into the 8*i* position with an occupancy of 1/4 (Figure 1, right). Within the *ab* plane, such atomic arrangements create shorter distances between the Sb atoms on the 4-fold degenerate position. In the case of Ce_2SbO_2 and Pr_2SbO_2 the shortest Sb−Sb distances are 3.23 Å. These Sb−Sb distances were viewed as evidence for

Received: October 13, 2011
Published: January 10, 2012

 © 2012 American Chemical Society dx.doi.org/10.1021/ja209652d | *J. Am. Chem.Soc.* 2012, 134, 1426−1429

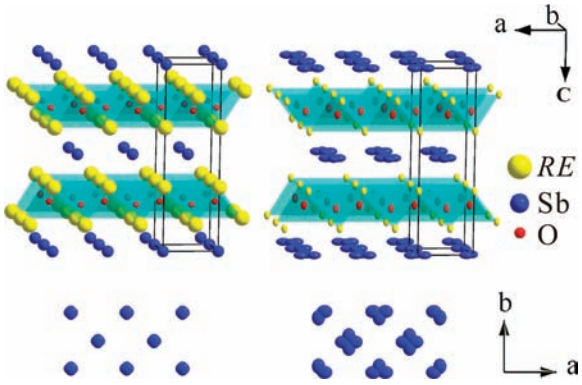

Figure 1. RE_2SbO_2 structural models with the Sb atom on the 2*a* (left) and 8*i* (right) positions.

Zintl-type Sb^{2-}–Sb^{2-} interactions.[10] Since the rare earth atoms were found in the 3+ oxidation state from the magnetic susceptibility measurements, and the bulk materials displayed a semiconductor type behavior,[9] the Zintl-type Sb^{2-}–Sb^{2-} dimers conveniently fit into the charge balanced formula, $RE^{3+}{}_2Sb^{2-}O^{2-}{}_2$. The X-ray single-crystal structural results obtained by us for other analogues of the RE_2SbO_2 series (*RE* = La, Nd, Sm, Gd, Ho, and Er) agree with the structural model proposed by Nuss and Jansen. As expected, the unit cell parameters decrease with the size of the *RE* elements (Supporting Information); however, the Sb–Sb atomic distances do not follow this trend. As shown in Figure 2, the

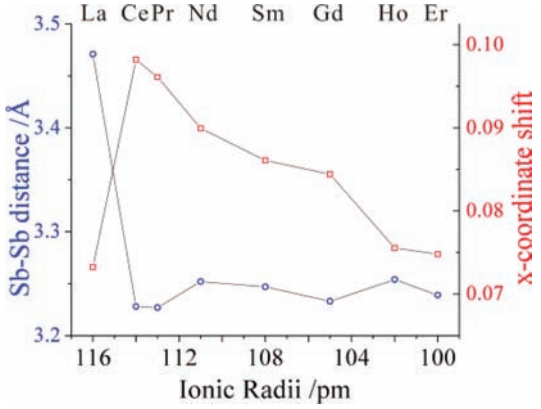

Figure 2. Shortest Sb–Sb distance (blue) and Sb *x*-coordinate shift (red) observed in the RE_2SbO_2 crystals with respect to the *RE* ionic radius.

Sb atoms in the large La_2SbO_2 unit cell do not shift along the *x*-direction enough to sustain effective Sb–Sb interactions. Instead, the Sb atoms in the La_2SbO_2 structure appear to be the most localized in the series. As a result, the closest Sb–Sb distance in the La_2SbO_2 structure is 3.471(6) Å. Throughout the rest of the series (Figure 2, left, blue), the Sb–Sb distances remain between 3.22 Å and 3.26 Å, as the reduction in the unit cell size is offset by smaller Sb *x*-coordinate shifts (Figure 2, right, red).

The electrical resistivity, Seebeck voltage, and thermal conductivity of the prepared RE_2SbO_2 samples were measured in the 2–400 K region on a QD PPMS instrument. As shown in Figure 3a, all the RE_2SbO_2 phases display a semiconductor-type behavior. La_2SbO_2 has the highest electrical resistivity, although the least effective Sb–Sb orbital overlap would imply

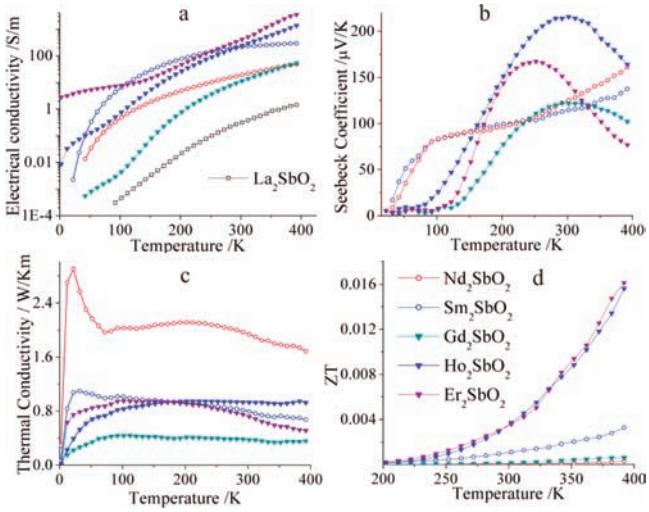

Figure 3. Electrical conductivities (a), Seebeck coefficients (b), thermal conductivities (c), and figure of merit *ZT* (d) of the RE_2SbO_2 compounds in the range of 0–400 K (200–400 K for *ZT*).

a metallic-type conductivity according to the electron-poor formula, $RE^{3+}{}_2Sb^{3-}O^{2-}{}_2$. The rest of the phases display electrical behaviors with different temperature dependence although their Sb–Sb distances are very similar.

In order to understand how the observed Sb atomic arrangement affects the physical properties of the RE_2SbO_2 compounds, the tight-binding, linear-muffin-tin-orbital calculations using the atomic sphere approximation (TB-LMTO-ASA)[11] were performed for Nd_2SbO_2. The ideal anti-$ThCr_2Si_2$-type structure (Figure 1, left) was used in the calculation, and a super structure was constructed to describe the disordered structure (Figure 1, right). The Nd_2SbO_2 unit cell was chosen for the calculation as it possessed the largest Sb *x*-coordinate shift. Both electronic band structures failed to describe the observed semiconductor-type electrical conductivity and suggested a metallic-type behavior (Supporting Information). Resembling the La_2BiO_2 band structure,[4] the Fermi level sits at the top of the valence band which is dominated by the Sb states, implying a metallic conductivity.

Since the Sb states in RE_2SbO_2 have the largest contribution at the vicinity of the Fermi level, the local atomic arrangement within the Sb layer will dictate the electrical properties of these phases. There are two interrelated structural parameters in the Sb layer, the Sb–Sb distances and the Sb site disorder, both of which are governed by the unit cell dimensions. However, for the first member of the family, La_2SbO_2, these parameters are different than for the rest of the group. The electronic structure of La_2SbO_2 conceivably resembles that of La_2BiO_2 more closely than the rest of the RE_2SbO_2 series, as the Sb site disorder is minor and the Sb–Sb distances are well above the single-bond values. Therefore, La_2SbO_2 can be considered as a Mott insulator, in which the poor overlap between Sb p-orbitals prevents the charge carrier propagation and, as a consequence, leads to the semiconductor-type conductivity.

In the rest of the RE_2SbO_2 compounds, the Sb–Sb distances are shorter and remain almost constant through the series. Although the Zintl-type Sb^{2-}–Sb^{2-} dimers could not be established from the structural analyses, previous studies[10,12] suggested that the long-range Sb–Sb interactions (~3.3 Å) may still influence the local electronic structure. In RE_2SbO_2, such interactions will cause energy separation between the bonding

dx.doi.org/10.1021/ja209652d | *J. Am. Chem.Soc.* 2012, 134, 1426–1429

and antibonding states of antimony dimers, thus introducing a pseudogap at the vicinity of the Fermi level. However, presence of a pseudogap alone is insufficient to elucidate the diverse electrical behaviors of the RE_2SbO_2 phases. RE_2SbO_2 (other than La_2SbO_2) possess significant Sb site disorder, which can be correlated to the Sb x-coordinate shift. According to Anderson,[13] a significant atomic disorder leads to the localization of states at the top and bottom of bands, where the density of states diminishes. In case of RE_2SbO_2, such localized states resulting from the Sb disorder would appear around the created pseudogap. Thus, in the RE_2SbO_2 series (other than La_2SbO_2), the observed semiconductor-type behaviors stem from the Anderson localization of the states within the pseudogap and around the Fermi level. A few arguments developed by Mott and Davis[14] will be used in the following discussion to reveal the nature of the observed electrical properties. Figure 4 shows three proposed charge carrier activation mechanisms: (a) hopping between localized states, (b) thermal activation into localized states, (c) thermal activation into nonlocalized states. While each of the three mechanisms may contribute to the measured electrical properties, the chemical pressure in the unit cell will determine which one is the dominant one by affecting the Sb site disorder.

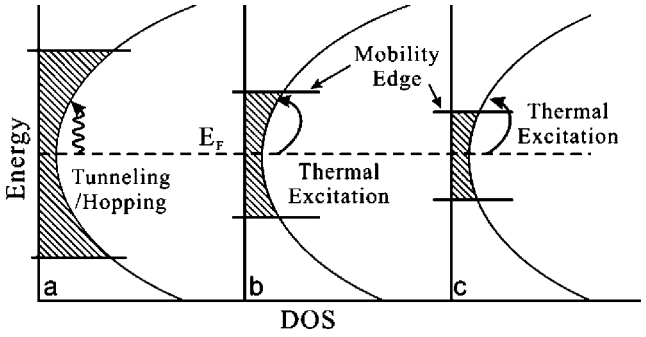

Figure 4. DOS at the Fermi level in the middle of a pseudogap. The shaded region represents localized states. The mobility edge is marked at the boundary between the localized and the nonlocalized states. Three charge carrier activation mechanisms are shown: (a) hopping between the localized states; (b) thermal activation into localized states; (c) thermal activation into nonlocalized states.

First of all, the energy range of localization is proportional to the extent of disorder, which is reflected by the Sb shifts (Figure 2). When unit cells are big as in Nd_2SbO_2 and Sm_2SbO_2, the Sb disorder is large, and electronic states within an extended energy range are localized (Figure 4a). Also because of the large atomic displacements, a range of Sb−Sb distances is accessible to the charge carriers. The combined outcome is a variable-range hopping (other than between the nearest neighbors), which allows charge carriers to propagate through the low-energy pathways at lower temperatures. Indeed, conductivity of Nd_2SbO_2/Sm_2SbO_2 obeys the variable-range hopping (VRH) formula, $\sigma \propto \exp(T^{-1/(d+1)})$, with d being the dimensionality.[15] A method of Hill[16] was employed to establish the dimensionality of the variable-range hopping. In the low-temperature region, the VRH conduction in the two compounds was confirmed by the linearity of the double logarithmic plot of the activation energy over temperature vs temperature (Supporting Information). Thus, the charge carriers are tunneling through the random potential created by localization, as shown in Figure 4a, i.e. they do not need to be thermally promoted to high-energy extended states. The VRH behavior is also manifested in the thermoelectric powers of Nd_2SbO_2 and Sm_2SbO_2 phases. At low temperatures, their Seebeck coefficients increase significantly, as the charge tunneling requires little thermal energy as long as a large number of hopping pathways are available for the charge carriers. However at high temperatures, thermoelectric power is rather weak as its value depends on the change in the chemical potential, which is small for a tunneling mechanism.

As the *RE* atomic size decreases, the Sb atoms become more spatially constrained toward the ideal 2*a* atomic site by the neighboring *RE* atoms. As a result, the energy range of localization decreases for the heavier rare earths. In the Ho and Er analogues, thermal excitation of charge carriers into the nonlocalized states in the conduction band becomes more dominant with increasing temperature (Figure 4c). Since the boundary (mobility edge) between the localized and nonlocalized states is associated with a change in the charge carrier mobility, μ, the electrical conductivities of the smaller RE_2SbO_2 phases are improved at higher temperatures (above 250 K). The Seebeck coefficients of Ho_2SbO_2 and Er_2SbO_2 are also enhanced (above 200K) as a change in the chemical potential originating from the carrier excitation process is greater than the energy range of the localized states.

The Gd_2SbO_2 phase, with an intermediate unit cell size, possesses a medium degree of the Sb displacement. As a result, the localized states are more extended than in the Ho/Er analogues, while the range of atomic distances available for the hopping process is narrower than that in the Sm/Nd analogues. Since there are fewer energy-equivalent electronic states for a charge carrier to tunnel into, the charge carriers are thermally activated. As a result, the Gd_2SbO_2 phase displays transport properties similar to those of the late members of the series. However, as the energy range of the localization is broad, the charge carriers are only excited into the localized states below the mobility edge (Figure 4b). The first consequence of such activation mechanism is a low electrical conductivity due to the low mobility. The less obvious outcome is a weaker thermoelectric power, since, according to Mott and Davis, only a part of the thermal activation energy contributes to the change in chemical potential, the rest is consumed by the hopping mechanism as the charge carriers propagate between the localized states.[14]

The Sb site disorder is also reflected in the thermal conductivities of the RE_2SbO_2 phases. Since the samples were cold pressed, a correction, representing experimental densities, was applied to the data following the method of Klemens.[17] As shown in Figure 3c, the RE_2SbO_2 compounds exhibit relatively low thermal conductivities, κ, which is likely due to the Sb disorder. The dimensionless figure-of-merit, ZT, which combines the three transport parameters, is presented in Figure 3d. As shown, the RE_2SbO_2 compounds with small *RE* elements have larger thermoelectric efficiencies (Figure 3d) as a result of the simultaneous enhancement in the Seebeck coefficient α and electrical conductivity σ.

In summary, the size of the rare earth elements was exploited as a chemical pressure to tune the Sb disorder in the RE_2SbO_2 phases. As a result, the RE_2SbO_2 materials with the same structure and similar charge carrier concentration exhibit a range of transport behaviors. The size of the unit cell governs the degree of the Sb site disorder and Sb−Sb distances, both of which determine a dominant charge carrier transport mechanism. Thus, rather than changing uniformly within the

dx.doi.org/10.1021/ja209652d | *J. Am. Chem.Soc.* 2012, 134, 1426−1429

series, the transport properties of some analogs are unique due to different activation processes. Consequently, the thermoelectric properties of these compounds are improved without compromising the electrical conductivity. The RE_2SbO_2 compounds are, by no means, the most efficient thermoelectric materials. However, this series illustrates possibilities of overcoming the classical challenges in thermoelectric research. Although the actual physics in these systems may be more complex, experimentally the decoupling of electrical conductivity and thermopower was indeed achieved by perturbing the charge carrier transport mechanism without modifying the carrier concentration.

■ ASSOCIATED CONTENT

Supporting Information

Crystal structure parameters, calculated electronic band structures, analysis of the variable range hopping. This material is available free of charge via the Internet at http://pubs.acs.org.

■ AUTHOR INFORMATION

Corresponding Author
mozhar@mcmaster.ca

■ ACKNOWLEDGMENTS

This work was supported by a Discovery Grant from the Natural Sciences and Engineering Research Council of Canada and by a grant from the ACS Petroleum Research Fund.

■ REFERENCES

(1) Tritt, T. M. *Science (Washington, D.C.)* **1996**, *272*, 1276−1277.
(2) Snyder, G. J.; Toberer, E. S. *Nat. Mater.* **2008**, *7*, 105−114.
(3) Sootsman, J. R.; Chung, D. Y.; Kanatzidis, M. G. *Angew. Chem., Int. Ed.* **2009**, *48*, 8616−8639.
(4) Mizoguchi, H.; Hosono, H. *J. Am. Chem. Soc.* **2011**, *133*, 2394−2397.
(5) Wang, P.; Forbes, S.; Kolodiazhnyi, T.; Kosuda, K.; Mozharivskyj, Y. *J. Am. Chem. Soc.* **2010**, *132*, 8795−8803.
(6) Hunter, B. A. H.; Howard, C. J. *Rietica*; Australian Nuclear Science and Technology Organization: Menai, Australia, 2000.
(7) Sheldrick, G. M.; Schneider, T. R. *Methods Enzymol.* **1997**, *277*, 319−343.
(8) Benz, B. *Acta Crystallogr.: Sect. B* **1971**, *27*, 853−854.
(9) Nuss, J.; Jansen, M. *J. Alloys Compd.* **2009**, *480*, 57−59.
(10) Papoian, G. A.; Hoffmann, R. *Angew. Chem., Int. Ed.* **2000**, *39*, 2409−2448.
(11) Andersen, O. K.; Pawlowska, Z.; Jepsen, O. *Phys. Rev. B* **1986**, *34*, 5253−5269.
(12) Xu, J.; Kleinke, H. *J. Comput. Chem.* **2008**, *29*, 2134−2143.
(13) Anderson, P. W. *Phys. Rev.* **1958**, *109*, 1492−1505.
(14) Mott, N.; Davis, E. A. *International Series of Monographs on Physics: Electronic Processes in Non-Crystalline Materials*; Oxford University Press; New York, 1978.
(15) Mott, N. F. *J. Non-Cryst. Solids* **1972**, *8−10*, 1−18.
(16) Hill, R. M. *Phys. Status Solidi A* **1976**, *35*, K29−K34.
(17) Klemens, P. G. *Int. J. Thermophys.* **1996**, *17*, 979−981.